

# Assessing the Accuracy of Different Solvation Models To Describe Protein Adsorption

Maria Ortega,<sup>†</sup> J. G. Vilhena,<sup>\*,†,‡,§</sup> Pamela Rubio-Pereda,<sup>¶,§</sup> P. A. Serena,<sup>¶</sup> and Rubén Pérez<sup>\*,†,||</sup>

<sup>†</sup>Departamento de Física Teórica de la Materia Condensada and <sup>||</sup>Condensed Matter Physics Center (IFIMAC), Universidad Autónoma de Madrid, E-28049 Madrid, Spain

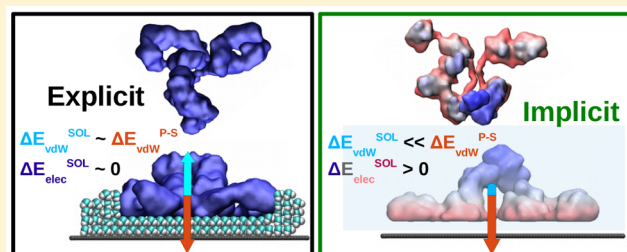
<sup>‡</sup>Department of Physics, University of Basel, Klingelbergstrasse 82, CH-4056 Basel, Switzerland

<sup>¶</sup>Instituto de Ciencia de Materiales de Madrid (ICMM), CSIC, c/Sor Juana Ines de la Cruz 3, E-28049 Madrid, Spain

<sup>§</sup>Centro de Investigación Científica y de Educación Superior de Ensenada 3918, 22860 Ensenada, Baja California, Mexico

## Supporting Information

**ABSTRACT:** In protein adsorption, the surrounding solvent has an important role in mediating protein–surface interactions. Therefore, it is of paramount importance that the solvent methods employed to model these kinds of processes are able to correctly capture the complex mechanisms occurring in the protein–water–surface interface. Here, we test the suitability of the two most popular implicit solvent methods based on the Generalized Born formalism to describe the adsorption process of the immunoglobulin G (IgG) on a hydrophobic graphene surface. Our results show that in both cases, IgG experiences an extreme and early (in less than 40 ns) unfolding as a result of the adsorption to the surface in contrast with previous experimental findings. A detailed energy decomposition analysis of explicit and implicit solvent simulations reveals that this discrepancy arises from the ill-characterization of two energy components in implicit solvent methods. These findings help to elucidate how implicit solvent models may be improved to accurately characterize the protein adsorption process.



## 1. INTRODUCTION

Protein adsorption has been a subject of great technological and fundamental interest.<sup>1,2</sup> Proteins constitute the largest and most widely employed class of biomolecules for surface functionalization. As a result, numerous biotechnology applications such as biocompatible implants, biosensors, and regenerative medicine<sup>1,3–5</sup> rely on the process of protein adsorption. This broad applicability has stimulated in the last years the development of many experimental studies addressed to achieve the challenge of visualizing biomolecules and their hydration layers<sup>6,7</sup> and controlling how a protein adsorbs to a surface.<sup>8–11</sup> However, the protein adsorption mechanism is not completely understood yet.<sup>2,12,13</sup> This results from the intrinsic nature of the process, which is driven by the interplay between both enthalpic and entropic forces.<sup>1</sup> The former are mostly composed by two components: the protein–surface interaction and the energy change due to protein’s and water’s structural rearrangement arising from its adsorption. The entropic forces, commonly known as hydrophobic forces, are, to a first approximation, a measure of how the disruption of the water–solute’s H-bond network induces or prevents the protein from adsorbing. How each of these kinds of interactions (enthalpic/entropic) contributes in the adsorption process is still a very challenging problem that is difficult to solve solely from the experiments. For this reason, atomistic computer simulations, such as classical

molecular dynamics (MD), have turned into an essential tool to shed light on the protein adsorption process. After all, these simulations provide atomistic-level insights into protein–substrate interactions, thus giving a deeper understanding and control on protein adsorption experiments.<sup>14,15</sup>

In MD simulations of the dynamics of biomolecules, a correct description of the solvent is needed.<sup>16</sup> The most direct way to properly account for the interaction between solvent–solute is by explicitly including all the water molecules present on the system. Nevertheless, this comes with a huge computational cost, as it increases the system size by at least 1 order of magnitude. This computational bottleneck has encouraged a fruitful development of a manifold of implicit-solvation methods.<sup>17–22</sup> In these methods, the solvent is represented by a continuous medium instead of individual explicit solvent molecules.<sup>16</sup> As a result, this class of approximations reduces the number of atoms of the solvated system (i.e., the simulation computational cost) and concurrently keeps a physically accurate description of the biological system of interest.<sup>15,23</sup> The suitability and efficiency of these methods has long been validated on MD simulations of biomolecules in solution.<sup>24–27</sup> However, it is still not clear if they are appropriate for studying

Received: October 19, 2018

Published: March 1, 2019

the protein adsorption process.<sup>16</sup> In fact, MD simulations of protein adsorption for the same or alike systems have shown qualitatively different results depending on the solvent method used. The works that use implicit solvent models<sup>28–34</sup> observe a severe degree of unfolding upon protein adsorption, whereas the works that use explicit water<sup>35–38</sup> observe the opposite. That difference seems to point out that the detailed role of the solvent in mediating protein–surface interactions can only be recovered by explicit-solvation methods.<sup>25</sup>

In this work, we compare the performance of explicit- and implicit-solvation methods to simulate the adsorption process of the immunoglobulin G protein (IgG) on a hydrophobic substrate such as graphene. In a previous work,<sup>39</sup> we experimentally validated that the IgG protein remains bioactive upon adsorption and corroborated the compatibility of explicit solvent MD simulation results with that experiments. Here we use two different implicit solvent methods (i.e., the HCT<sup>40</sup> and OBC<sup>41</sup> methods) to simulate the IgG adsorption process on graphene. The results of both simulations clearly show that the IgG denatures upon adsorption, which contrasts with previously reported experimental and explicit solvent results.<sup>39</sup> To understand the differences observed between explicit and implicit solvent results, we also perform a detailed analysis of the evolution of the different energy components of the system for both explicit and implicit solvent simulations. This analysis highlights the importance of the entropic effects when a protein adsorbs on a hydrophobic surface and shows the two factors that lead to the unfolding of the protein when implicit solvent is used. First, implicit-solvation methods underestimate the cost of breaking both protein and substrate solvation shells, prompting an instantaneous adsorption process. In addition, as the protein adsorbs, the implicit solvent description of the loss of solute–solvent interaction leads to large electrostatic energy unbalances inside the protein, which causes its unfolding. Therefore, with this work, we pave the way for using implicit-solvation methods to describe the adsorption process of biomolecules as we unravel the characteristics of these methods that must be corrected to that end.

## 2. SIMULATION METHODS

**2.1. System Structure.** The protein structure of the IgG, composed of 1316 amino acids and 2 glycan heteropolymer chains, was obtained from the Protein Data Bank (PDB ID: 1IGT<sup>43</sup>). It is composed of four peptide chains (two heavy chains and two light chains, see Figure 1a) arranged in a Y-shape. Protons were added to the protein structure according to the calculated ionization states<sup>44</sup> of its titratable groups at a blood pH of 7.4, resulting in a zero net charge. The IgG was then centered on top of a 20 × 20 nm<sup>2</sup> two-layer graphene slab with A–B stacking. We have oriented the IgG flat on the surface (Figure 1b,c). The initial distance between the lowest protein atom and the first graphene layer was 10 Å (Figure 1b). All graphene atoms were set to be neutral, and the bottom graphene layer of the slab was kept fixed during all simulations. This setup mimics the typical configuration in many adsorption experiments where a graphene layer is supported on an inert, mechanically rigid substrate.

**2.2. Force Fields.** The protein and the oligosaccharide were modeled by the AMBERff99SB<sup>45</sup> and Glycam04<sup>46</sup> force fields, respectively. These force fields successfully sample the conformational space that an antibody explores in aqueous solution<sup>47</sup> and when it is adsorbed to surfaces.<sup>39</sup> The carbon atoms of the three-layered graphene were modeled by the OPLS

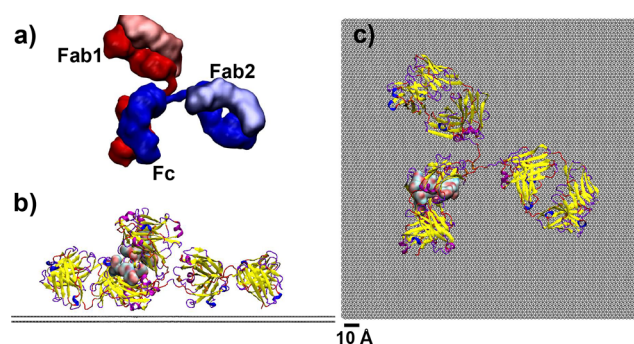


**Figure 1.** Initial configuration of the system IgG–graphene. (a) Representation of the IgG molecule. Its four peptide chains have been marked with four different Connolly surfaces:<sup>42</sup> the two light chains<sup>43</sup> are represented with metallic-pastel colors, and the two heavy chains<sup>43</sup> are represented with opaque colors. The three fragments that compose the IgG (i.e., Fc (fragment crystallizable region) and Fab1/2 (fragment of antigen binding 1 and 2)) are labeled accordingly. (b) Side and (c) top views of the initial IgG–graphene configuration. The IgG is represented with its secondary structure:  $\beta$ -sheets (yellow),  $\alpha$ -helix (purple), 310-helix (dark-blue), turns (violet), and random coils (red). The position of the two glycan chains has been highlighted with a Connolly surface.<sup>42</sup> The disulfide bridges of the protein are also marked with an orange bond. The graphene has been represented in gray color.

aromatic carbon force field present on AMBER’s generalized force field.<sup>48</sup> This force field is known to properly describe graphene’s mechanical and hydration properties<sup>49</sup> as well as its interaction with biological systems.<sup>47,50</sup> Moreover, recent joint experimental and theoretical work showed that this force field is capable of not only correctly characterizing the adsorption process of the immunoglobulin G onto a graphene surface<sup>39</sup> but also properly describing the graphene tribological properties in UHV and water conditions.<sup>51</sup>

**2.3. Implicit Solvent Methods.** For implicit simulations, we have used two different methods, HCT<sup>40</sup> and OBC,<sup>41</sup> both based in the GB/SA formalism. In this formalism, the total solvation free energy of a molecule is given by<sup>41</sup>

$$E_{\text{SOL}} = E_{\text{SOL}(el)} + E_{\text{SOL}(nonel)} \quad (1)$$

where  $E_{\text{SOL}(el)}$  accounts for the variation in the electrostatic interaction between the molecule atoms resulting from the presence of a continuum dielectric solvent, and  $E_{\text{SOL}(nonel)}$  includes both the solute–solvent vdW interactions and the hydrophobic effects. This second term is defined to be proportional to the total solvent-accessible surface area (SA) of the molecule (i.e.,  $E_{\text{SOL}(nonel)} = \gamma \text{SA}$ ).<sup>40,41,52,53</sup> As shown later in this work, (Sec 3.2) the contribution of this term to the total solvent energy is negligible. Considering that, to reduce the simulation cost<sup>54</sup> and facilitate the interpretation of the results, we have not included this term in our implicit solvent simulations.

The first term,  $E_{\text{SOL}(el)}$ , is computed using the Generalized Born (GB) approximation,<sup>41</sup> which describes the screening of the electrostatic interaction of two atoms of the molecule ( $q_i, q_j$ ) resulting from the presence of a pure solvent with high dielectric value  $\epsilon_\omega$  (80 for water at 300 K) as

$$E_{\text{SOL}(el)} = E_{\text{GB}} = -\left(\frac{1}{2} - \frac{1}{2\epsilon_\omega}\right) \sum_{ij} \frac{q_i q_j}{r_{ij} \sqrt{1 + \frac{R_i R_j}{r_{ij}^2} e^{-r_{ij}^2/4R_i R_j}}} \quad (2)$$

where  $r_{ij}$  is the distance between atoms  $i$  and  $j$ , and  $R_i$  is the effective Born radii of atom  $i$ . This radii reflects the degree of burial of the atom  $i$  inside the molecule (i.e., the deeper is the atom inside the molecule, the higher the radii is). Therefore, according to eq 2, the atoms that are nearer to the molecular surface have a bigger contribution to  $E_{\text{SOL}(el)}$  than the atoms that are buried inside the molecule.

The difference between the two implicit solvent models here used is in the effective Born radii definition. In the HCT model,<sup>40</sup> for computing the Born radii, the molecules that constitute the solute are defined as a group of vdW spheres with dielectric constant unity. The rest of the space (i.e. all the space that is not occupied by a sphere) has the high dielectric value of the media. The Born radii for each atom is then computed as

$$R_k^{-1} = \rho_k^{-1} - \int_{\rho_k}^{\infty} \frac{dr}{r^2} H_k(r, \{\rho_{k'}, r_{kk'}\}_{\text{all } k'}) \quad (3)$$

where  $H_k$  is the fraction of the eclipsed surface area of a sphere of radius  $r$  centered at atom  $k$  with vdW radius  $\rho_k$  when it is surrounded by spheres of radius  $\rho_{k'}$  at a distance  $r_{kk'}$ . In the OBC<sup>41</sup> model, the authors changed this original Born radii definition, because it overestimates the solvation energy for deeply buried atoms. This overestimation is caused by the presence of artificial highly dielectric crevices in internal regions of the solute, in which actually the solvent has been completely expelled.<sup>52</sup>

**2.4. Explicit Solvent Model.** For explicit solvent simulations, the TIP3P water model<sup>55</sup> has been chosen. This water model not only suitably describes the interaction of water with proteins but also graphene's wetting properties.<sup>30</sup> We have used periodic boundary conditions with a cubic unit cell that extends 20 Å above/beyond the molecule in the three directions. In order to solvate the system, this unit cell has been filled up with water molecules, placed in such a way that the minimum solute–water distance is 1 Å. This results in a system composed by ~450.000 atoms. Note that in the implicit solvent simulations, the system is only composed by ~60.000 atoms.

**2.5. MD Parameters.** We used the AMBER12 software suite<sup>56</sup> with NVIDIA GPU acceleration.<sup>57,58</sup> For explicit solvent simulations, Particle Mesh Ewald<sup>59,60</sup> (with a real-space cutoff of 10 Å) was used to account for long-range electrostatic interactions. Van der Waals interactions were truncated at the real-space cutoff. The SHAKE<sup>61</sup> algorithm was used to constrain bonds containing hydrogen atoms, thus allowing us to use an integration time step of 2 fs. Coordinates were saved every 1000 steps. A constant temperature of 300 K was ensured in all the simulations by means of a Langevin thermostat<sup>62</sup> with a friction coefficient  $\gamma = 1 \text{ ps}^{-1}$ . A Berendsen barostat<sup>63</sup> with a relaxation time of  $t_p = 1 \text{ ps}$  was used to keep the pressure constant at 1 atm during equilibration of the system to a consistent density value at 300 K. This is a preliminary step in the preparation of our production constant volume (NVT) simulations. In spite of the known limitations of this barostat (it suppresses pressure fluctuations more drastically compared to what is expected in the true isobaric–isothermal ensemble), ref 64 shows that it can be efficiently used to equilibrate the system density. We have explicitly tested this point by analyzing the density evolution in that constant pressure (NPT) preliminary stage using the Monte Carlo barostat.<sup>65</sup> Figure S1 shows that the difference between the final density values obtained with these two methods is less than 1%, what reinforces the validity of the Berendsen barostat for equilibrating the system density.

For implicit solvent simulations, we do not use periodic boundary conditions (i.e. the long-range energetic contributions are not truncated). We also use the SHAKE<sup>61</sup> algorithm and keep a constant temperature using a Langevin thermostat<sup>62</sup> with the same conditions employed in explicit solvent simulations.

**2.6. Protein Adsorption Protocol.** Our simulation protocol is composed by three main stages. In the first stage, we performed an energy minimization to prevent steric clashes, using a combination of steepest descent and conjugate gradient methods. During this process, we kept weak restraints at the protein backbone and graphene substrate. In the second stage, we heated up the system from 0 to 300 K while restraining the position of the protein backbone and the first graphene layer. In the explicit solvent simulation, we use constant pressure conditions (NPT) during this stage. Once these two preliminary stages had been performed, we started with the adsorption process of the protein, in which we let the protein freely adsorb to the substrate. This stage can be divided in three parts. First, we performed a 10 ns simulation, in which the protein is free to adsorb to the nearby substrate. In the explicit solvent simulation, we use volume constant periodic conditions (NVT) during this first phase. Next, we performed a steered molecular dynamics (SMD) simulation to enhance the adsorption process. This SMD process consists of moving toward the surface a selected group of atoms at a constant velocity of 5 Å/ns via a harmonic restraint (with  $k = 50 \text{ kcal/mol}$ ). This restraint is only applied to the  $\alpha$ -carbons belonging to 16 cysteine residues evenly distributed over the protein. The disulfide bonds formed between cysteine residues play an important role in the protein stability. In Figure S2, we show that restraining these  $C_\alpha$  atoms does not induce changes in the IgG protein structure. Finally, once the protein has reached the surface, a long MD stage of up to 140 ns in an NVT ensemble was carried out for the explicit solvent simulation. In the case of implicit solvent simulations, the early high degree of unfolding justified stopping the simulations at 40 ns.

**2.7. Data Analysis.** In order to characterize the protein–surface adsorption process, we have used the CPPTRAJ tools within the AMBER package.<sup>66</sup> We have evaluated the following quantities: root-mean-square deviation (RMSD) of the protein backbone and domains,<sup>66</sup> the evolution of the secondary structure<sup>67,68</sup> of the protein, and the evolution of the contact-surface area (CSA) between the protein/substrate. The latter is calculated using the following definition

$$CSA(t) = \frac{1}{2}(SA_p(t) + SA_s(t) - SA_{p-s}(t)) \quad (4)$$

where the time dependent solvent-accessible surface area  $SA(t)$ <sup>42</sup> was calculated for protein ( $SA_p(t)$ ), substrate ( $SA_s(t)$ ), and protein–substrate ( $SA_{p-s}(t)$ ).

**2.8. Energy Decomposition.** As the graphene atoms are not charged, the only enthalpic interaction between protein and substrate is the van der Waals interaction (vdW). When we refer here to *van der Waals interaction*, we mean the interaction described by the Lennard-Jones potential, which includes both the van der Waals attractive effects and the Pauli repulsive effects. We computed this interaction energy as a function of time via an energy decomposition on each frame of our MD trajectories. As a result, the protein–surface interaction is given by

$$E_{\text{total}}^{P-S}(t) = E_{\text{vdW}}^{P-S}(t) = E_{\text{vdW}}^{P+S}(t) - E_{\text{vdW}}^P(t) - E_{\text{vdW}}^S(t) \quad (5)$$

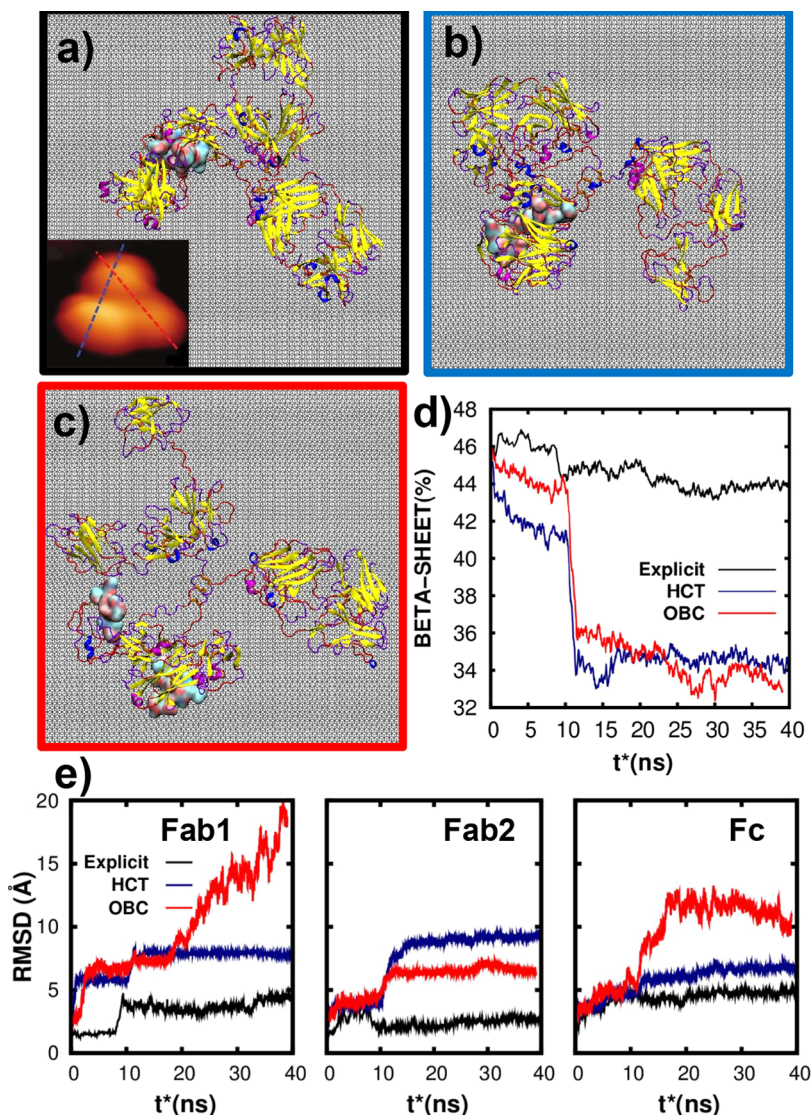


**Figure 2.** Structural changes of the IgG during the adsorption process. Top views of the IgG–graphene configurations obtained at the end of the simulation using (a) explicit TIP3P,<sup>55</sup> (b) HCT implicit,<sup>40</sup> and (c) OBC implicit<sup>41</sup> methods. The inset in a shows an AFM image of the IgG antibody adsorbed in graphene that was published in ref 39. The color representation used for the system protein–substrate is the same as in Figure 1. (d) Time evolution of the percentage of  $\beta$ -sheet content of the IgG in the adsorption process using the explicit solvent method (black),<sup>55</sup> HCT implicit method<sup>40</sup> (blue), and the OBC implicit method<sup>41</sup> (red). The time of simulation for the explicit solvent case has been rescaled using the relation  $t^* = t_{sim}/4.6$ . (e) Time evolution of the RMSD for the atoms belonging to the two antigen-binding fragments (Fab1 and Fab2) and the Fc fragment using the three different solvent methods. The color and time scales are the same as in panel d. The inset in panel a is reproduced by permission of The Royal Society of Chemistry. Copyright 2016.

where  $E_{vdW}^{P+S}(t)$  stands for the vdW energy of the combined protein + substrate system, and  $E_{vdW}^P(t)$  and  $E_{vdW}^S(t)$  are the vdW energies of the isolated protein and substrate, respectively. Additionally, to elucidate the role of the solvent in the adsorption process when explicit solvent is used, we have calculated also the interaction of each individual system (i.e., the protein and the substrate) with the water molecules. These two magnitudes are computed analogously to  $E_{vdW}^{P-S}$

$$E_{total}^{W-P}(t) = E_{total}^{W+P}(t) - E_{total}^P(t) - E_{total}^W(t) \quad (6)$$

$$E_{total}^{W-S}(t) = E_{total}^{W+S}(t) - E_{total}^S(t) - E_{total}^W(t) \quad (7)$$

where  $E_{total}^{W+P(S)}(t)$  stands for the total energy of the combined water + protein(surface) system, and  $E_{total}^{P(S)}(t)$  and  $E_{total}^W(t)$  are the total internal energies of the isolated protein(substrate) and water systems, respectively. The water–protein interaction is a

combination of electrostatic and vdW effects (i.e.  $E_{total}^{W-P}(t) = E_{el}^{W-P}(t) + E_{vdW}^{W-P}(t)$ ) whereas the water–substrate interaction is a pure vdW interaction, as the graphene atoms are not charged (i.e.  $E_{total}^{W-S}(t) = E_{el}^{W-S}(t)$ ).

### 3. RESULTS AND DISCUSSION

**3.1. Structural Dynamics of the Adsorption Process: Comparison between Different Solvent Models.** Explicit solvent simulations results (Figures 2a and S3) show that, upon adsorption, the IgG keeps its three-lobe structure, in which each lobe corresponds to a fragment (Fab1/2, Fc). This structure is also clearly distinguished in previously reported AFM experiments of IgG molecules adsorbed over graphene<sup>39</sup> (see inset of Figure 2a). Furthermore, these experiments<sup>39</sup> show that one of the fragments is slightly higher than the other two. This is reflected by a brighter color of one of the lobes on the image

shown in the inset of Figure 2a. This observation is fully consistent with our MD explicit solvent results, as in our simulations, the Fc fragment is slightly higher than the Fab fragments (see side views in Figure S3). Moreover, the interdomain distances obtained in the AFM experiments (i.e.,  $d_{Fab1-Fab2} \approx 7.8$  nm and  $d_{Fab1-Fc} \approx 6.7$  nm) are also in good agreement with explicit solvent MD simulations<sup>39</sup> as shown in Figure S4. Everything considered, we may conclude that the IgG adsorbed structure obtained in explicit solvent simulations is in excellent agreement with that obtained in AFM experiments.<sup>39</sup>

A key point concerning the IgG adsorption to surfaces is whether it preserves its biological functionality (i.e., the ability to bind specifically to an antigen via the Fab fragments). We have previously confirmed<sup>39</sup> that this is the case for IgG adsorbed to graphene via single molecule force spectroscopy experiments. This bioactivity can only occur if and only if the variable region of the Fab fragments preserves its tertiary structure.<sup>69</sup> Our explicit solvent simulation results corroborate this, as the relative position of the two chains conforming each Fab fragment is preserved upon adsorption (Figure S3).

In Figure 2b,c, we report the final adsorption configurations obtained for both implicit solvent methods considered here (i.e., HCT<sup>40</sup> and OBC).<sup>41</sup> Concerning the HCT<sup>40</sup> method results (Figure 2b), we may perceive three major structural changes. The first is the major unfolding of the Fab fragments, the Fab2 being the most affected. Second, the collapse of the Fc fragment occurs due to the clustering of the glycan chains located in the core of the Fc. The third and last aspect is the clustering of the Fab1 and Fc fragments, most clearly seen in Figure S3, which is driven by a self-interaction of one of the heavy chains of the IgG (shown in opaque red in Figure S3). These three changes of the IgG tertiary structure do not happen when we simulate the dynamics of this protein free in solution using the HCT implicit-solvation method (Figure S5). Considering now the OBC<sup>41</sup> results (Figure 2c), we note that the IgG also suffers a major unfolding due to adsorption, even more pronounced than the unfolding obtained using the HCT method. The severe loss in the secondary and tertiary structures of Fc and Fab1 fragments leads to a spreading of the IgG over the surface. This is not observed when we simulate the IgG dynamic free in solution using the OBC implicit solvent, as shown in Figure S5. Additionally, as is better shown in Figure S3, the two glycan chains of the Fc fragment separate during the OBC implicit solvent simulation.

Both OBC and HCT structural changes are at odds with the AFM experiments previously mentioned.<sup>39</sup> They are unable to reproduce the three-lobe structure and the compact adsorption area of the IgG obtained in AFM experiments<sup>39</sup> (Figure S4). In addition, the major degree of unfolding of the Fab fragments observed in both implicit solvent simulations is incompatible with the bioactivity of the IgG observed experimentally.<sup>39</sup> This seems to indicate that OBC and HCT implicit methods do not correctly describe the adsorption process of the IgG.

All these structural changes can be quantitatively confirmed by analyzing the evolution of the RMSD deviation of each IgG fragment, which is shown in Figure 2e. Explicit solvent simulations show RMSD values below 5 Å for all fragments, highlighting the strong similarity of the final adsorbed configurations with its crystal structure.<sup>43</sup> This is not the case for implicit solvent results, which show for the three fragments larger RMSD values than using explicit solvent. In fact, for both implicit solvent methods, the Fab1 fragment loses more tertiary structure (RMSD  $\approx 7$  Å) in the initial 10 ns than in 150 ns of the

explicit solvent simulation. Similar processes may be observed in the other fragments of the molecule, evidencing the striking difference between implicit and explicit solvent methods in describing the adsorption process.

When comparing OBC<sup>41</sup> with HCT<sup>40</sup> MD results, we observe that overall, the former leads to a larger structural change. In particular, in Figure 2e, we see that the RMSD of Fab1 and Fc is not stabilized in 40 ns of OBC simulation, indicating that further unfolding would occur. Furthermore, the RMSD is above 10 Å for two fragments (Fc, Fab1), which is consistent with the almost complete loss of its tertiary structure shown in Figure 2c. Considering that the sole difference between both implicit solvent methods is the electrostatic solvent energy contribution (eq 2), these differences seem to suggest that the observed protein unfolding upon adsorption may be related with the description of that energy component, in particular, with the definition of the degree of burial<sup>41</sup> of the amino acids at the protein–surface interface.

To quantify the loss of protein secondary structure resulting from the adsorption process, we now analyze the evolution of the  $\beta$ -sheet content (Figure 2d), which is the most abundant secondary structure in the IgG. The explicit solvent simulations predict a decrease of the  $\beta$ -sheet content below 2%, which is consistent with the preservation of the functionality of the protein<sup>69</sup> reported experimentally. However, implicit solvent simulations predict a  $\beta$ -sheet content decay higher than 10%, balanced with an increase of the content of random coils (Figure S6). In the first 10 ns of implicit solvent MDs, the protein lost more  $\beta$ -sheet content than in 150 ns of explicit solvent simulation. Moreover, when we enhance the adsorption,  $\beta$ -sheet content decreases even further as a consequence of protein approaching surface. As can be also observed in the RMSD evolution, the major structural rearrangement occurring during the adsorption seems to be dramatically promoted in protein–surface contact regions. This protein-structural instability promoted by the contact is in agreement with data shown in Figure S3 and shall be the subject of a thorough discussion in following subsections.

In summary, upon analysis of the tertiary structure, RMSD, and secondary structure shown in Figure 2, we may conclude that OBC and HCT methods predict a major structural rearrangement of the IgG upon adsorption to graphene. This result is independent of the protein orientation upon the surface, as we observe a similar structural distortion for another initial protein configuration (Figure S7). Altogether, this is incompatible<sup>69</sup> with the preservation of both structural and biofunctionality shown by the experimental observations.<sup>39</sup> Therefore, our results firmly confirm that improvements on OBC and HCT implicit methods are required in order to correctly describe the adsorption process of the IgG.

**3.2. Effect of the Non-Electrostatic Solvation Contribution ( $E_{SOL(none)}$ ) in the Adsorption Process.** In a previous work,<sup>70</sup> similar results were found for a completely different protein, the bovine serum albumin (BSA). Proteins such as antibodies and serum albumin are different in size, secondary structure composition, and net charge. Despite these differences, implicit solvent simulations predicted also a major BSA unfolding upon its adsorption,<sup>70</sup> contrasting with both explicit solvent simulations<sup>70</sup> and recent experimental reports.<sup>71</sup> Therefore, the observed IgG unfolding upon adsorption in implicit solvent simulations seems not to be a specific feature of this protein but a general characteristic of implicit solvent methods. In ref 70, we speculated that such a degree of unfolding

could be attributed to a strong energy gradient that arises from an abrupt change of the non-electrostatic solvation contribution ( $E_{SOL(nonel)}$ ) when the protein contacts the surface. In what follows, we test the validity of this assumption through a detailed energy decomposition analysis.

In Figure 3a, we plot the energetic change of the protein–substrate system ( $\Delta E^T$ ) as a function of the distance between

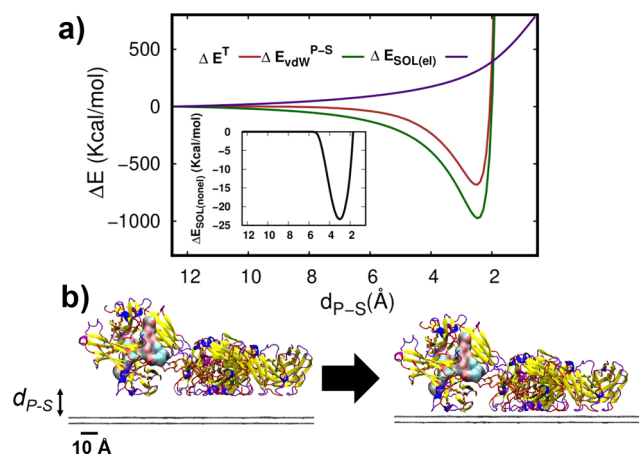


**Figure 3.** Description of the  $\Delta E(d_{p-s})$  with implicit solvent methods. (a) Change of the total interaction energy (red) with the protein–surface distance ( $d_{p-s}$ ) using the HCT implicit<sup>40</sup> solvent method. The contributions to this change are the protein–substrate interaction (green), the electrostatic solvation contribution (purple), and the non-electrostatic solvation contribution (inset, in black). The distance  $d_{p-s}$  is defined as the  $z$ -coordinate of the lowest hydrogen atom of the proline 889, considering that the upper graphene layer is at  $z = 0$ . (b) Representation of the system configuration used to compute this energy change.

them ( $d_{p-s}$ ) using the HCT method (see Figure S8 for OBC results). To compute it, we initially placed the IgG at  $d_{p-s} \approx 12.5$  Å, and we brought it closer to the surface in steps of 0.1 Å (Figure 3b). The total energetic change from its initial value (i.e.,  $E^T$  at  $d_{p-s} \approx 12.5$  Å) is evaluated in all intermediate steps of  $d_{p-s}$ . We also compute the different contributions to the total energy change

$$\Delta E^T = \Delta E_{vdW}^{P-S} + \Delta E_{SOL(el)} + \Delta E_{SOL(nonel)} \quad (8)$$

where  $E_{vdW}^{P-S}$  is the graphene–protein van der Waals interaction energy,  $E_{SOL(el)}$  is the electrostatic component of the solvation energy (eq 2), and  $E_{SOL(nonel)}$  is the non-electrostatic contribution to the solvation energy. In Figure 3a, we observe that the change of the total energy of the system ( $\Delta E^T$ ) strongly depends on the protein–surface separation. From here on, we shall focus only its evolution at  $d_{p-s} \geq 2.5$  Å, where the adsorption process is energetically favorable ( $\Delta E^T < 0$ ). For a matter of convenience, we shall call this distance range the *adsorption regime*. At last, it is important to remark that the coordinates of the protein were kept fixed in all steps (i.e., not allowing for the structural reorganization of the protein). The protein configuration used is the final adsorption configuration obtained in explicit solvent simulations, as it is the folded configuration that leads to the largest SA change when the protein contacts the surface.

First we consider the change of the non-electrostatic solvation contribution ( $\Delta E_{SOL(nonel)}$ ) as a function of  $d_{p-s}$  (inset of Figure 3a). From here, we observe not only that  $E_{SOL(nonel)}$  changes

smoothly with  $d_{p-s}$  but also its contribution to the total energy change is negligible (i.e.,  $\Delta E_{SOL(nonel)} = 3.5\% \Delta E^T$ ). These two aspects support that  $E_{SOL(nonel)}$  plays a minor role, if at all, in the adsorption process. Therefore, this shows that our previous conjecture<sup>70</sup> is wrong, as  $\Delta E_{SOL(nonel)}$  alone cannot account for the spurious protein unfolding observed in implicit solvent simulations.<sup>34,70</sup> Note that this negligible contribution of  $\Delta E_{SOL(nonel)}$  to the total energy change happens in a simulation designed to maximize it (i.e., we picked the IgG folded structure with the largest CSA, which should result in the largest  $\Delta E_{SOL(nonel)} = \gamma^* CSA$ ).

We now focus on the change of the other energy components:  $E_{vdW}^{P-S}$  and  $E_{SOL(el)}$ . First, we consider the van der Waals protein–surface interaction ( $E_{vdW}^{P-S}$ ) evolution. From Figure 3a, we observe that this energy component accounts for most of the variation in the total energetic change, as it decreases by  $E_{vdW}^{P-S} \approx 1000$  kcal/mol. Thus, it follows that this attractive interaction is the main driving force of this process. Second, we consider the variation of the  $E_{SOL(el)}$ , which for protein adsorption on neutral surfaces, it represents the solvent electrostatic screening within the protein. Note that this component is the sole difference between OBC (Figure S8) and HCT (Figure 3) methods, and thus, it fully accounts for the slightly different adsorptions obtained with them. From these figures, we see that  $\Delta E_{SOL(el)}$  is contributing significantly to the total energy change, namely, by 30%. In particular, for HCT/OBC, we observe that  $E_{SOL(el)}$  increases by 300/400 kcal mol<sup>-1</sup> during the adsorption, which highlights the highly repulsive nature of this interaction. Additionally, this variation shows that when approaching the surface, the protein is losing a significant amount of its electrostatic screening, which shall certainly affect its internal stability.

**3.3. vdW Interaction: The Cost of Breaking the Solvation Shell and Its Importance.** In Figure 4a, we show the variation of the vdW protein–substrate interaction during the adsorption time ( $\Delta_t E_{vdW}^{P-S}$ ) for all the solvents considered here. Note that, henceforth, the results presented always refer to the MD simulations characterized in Sec 3.1. From Figure 4a, we observe that in all cases  $\Delta_t E_{vdW}^{P-S} < 0$ , that is, the vdW protein–substrate interaction favors the adsorption process regardless of the solvent method used. In contrast with this similarity, two major differences may also be noticed when comparing explicit and implicit solvent results. First, at the end of the adsorption process, we observe that  $|\Delta_t E_{vdW}^{P-S}|$  is  $\sim 5$  times larger in implicit solvent simulations as compared to the explicit solvent simulations. It is worth mentioning that, among implicit solvent methods, the largest energy is obtained with the OBC method, which is also the one where a larger protein unfolding is observed. The second major difference between implicit and explicit solvent results concerns the variation rate of  $E_{vdW}^{P-S}$  in the initial 10 ns stage prior to the enhanced adsorption protocol. In explicit solvent simulations, we observe a smooth decrease of  $E_{vdW}^{P-S}$  as the protein approaches the surface. This is at odds with OBC/HCT results, where we observe an initial abrupt change of this interaction. In fact, in explicit solvent simulations at the end of the whole adsorption process ( $\Delta t = 150$  ns), the total  $\Delta_t E_{vdW}^{P-S}$  is much smaller than the corresponding change during the initial 10 ns of implicit solvent simulations.

In order to understand the origin of the different  $\Delta_t E_{vdW}^{P-S}$  obtained at the end of each simulation, we now analyze how this interaction is correlated with the CSA. From Figure 4b, we observe that  $\Delta_t E_{vdW}^{P-S}$  depends linearly on CSA, with a similar slope for all the solvent methods considered here. Moreover, when computing the slope, we obtain  $\Delta_t E_{vdW}^{P-S} / \Delta CSA \approx 32$  kcal

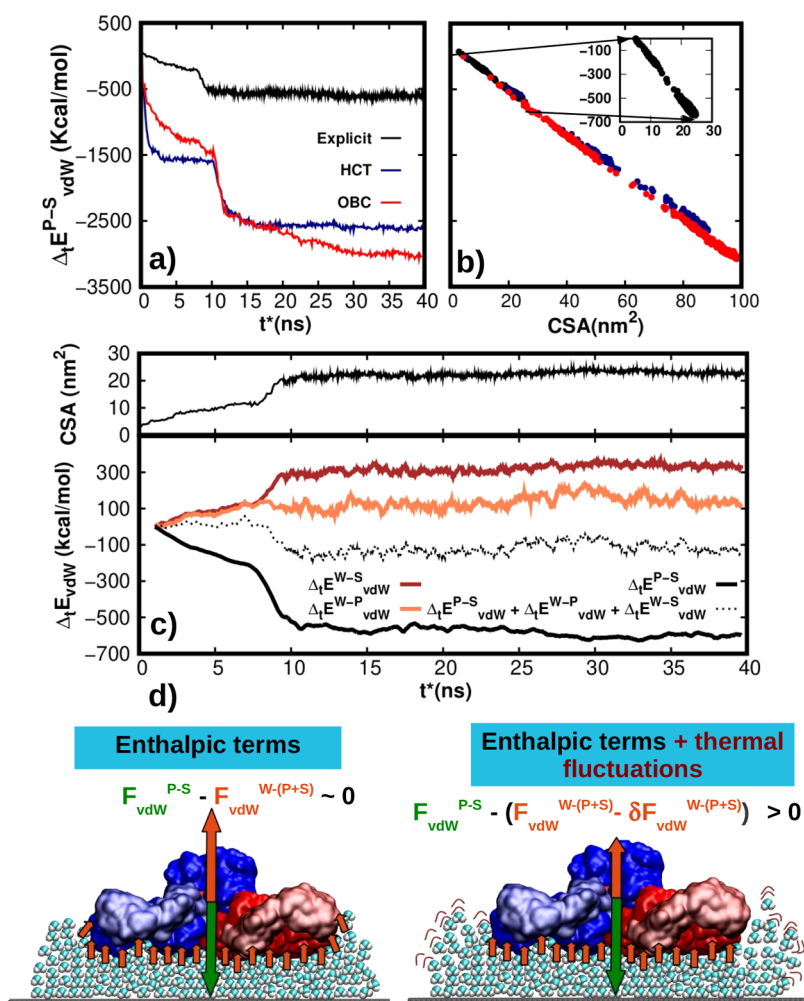


**Figure 4.** Role of the vdW interaction. (a) Variation of the interaction energy between the protein and the substrate ( $\Delta_t E_{vdW}^{P-S}$ ) during the simulation time for the whole adsorption process. The obtained results using the TIP3P explicit solvent<sup>55</sup> (black), the HCT implicit<sup>40</sup> solvent (blue), and the OBC implicit<sup>41</sup> solvent (red) are all shown. (b) Evolution of the interaction energy between the protein and the substrate with the contact-surface area (CSA) for the three solvent methods used: explicit<sup>55</sup> (black), HCT implicit<sup>40</sup> (blue), and OBC implicit<sup>41</sup> (red). The evolution of  $\Delta_t E_{vdW}^{P-S}$  with CSA using explicit solvent has been also represented in the inset. (c) Time evolutions of the CSA (top panel) and of the sum of all intermolecular vdW interaction energies (bottom panel, black dashed line) using explicit solvent. These interaction energies are the vdW water–protein interaction  $E_{vdW}^{W-P}$  (orange), the vdW water–substrate interaction  $E_{vdW}^{W-S}$  (brown), and the vdW protein–substrate interaction  $E_{vdW}^{P-S}$  (black). The time of simulation for the explicit solvent case has been rescaled in all the figures using the relation  $t^* = t_{sim}/4.6$ . (d) The enthalpic vdW energy balance between the attractive protein–surface interaction and the force opposing the solvent squeezing out is broken by the water thermal fluctuations, which lead to transient force unbalances and, ultimately, to protein adsorption (see text).

$\text{mol}^{-1} \text{nm}^{-2}$  (Figure S9), which is in excellent agreement with vdW interaction energies per unit area obtained in gold-standard quantum chemistry simulations ( $10\text{--}100 \text{ kcal mol}^{-1} \text{ nm}^{-2}$ ).<sup>72</sup> Besides the obvious conclusion that regardless of the solvent method used, the interaction  $E_{vdW}^{P-S}$  is computed similarly, this result highlights that implicit solvent methods have a larger  $\Delta_t E_{vdW}^{P-S}$  only because at the end of the adsorption process, the CSA is also larger. Thus, larger  $\Delta_t E_{vdW}^{P-S}$  is solely a consequence, and not the origin, of why different solvation methods result in very different final adsorption configurations. Additionally, this indicates that to trace the origin of these differences, we must understand why CSA increases more easily in implicit solvent methods as compared to explicit ones.

The slower rate of CSA obtained in explicit solvent simulations can be understood in light of the time evolution of all intermolecular vdW interactions ( $\Delta_t E_{vdW}$ ) shown in Figure 4c. There we observe that in the initial free adsorption regime ( $t < 10 \text{ ns}$ ), the attractive protein–substrate interaction energy

( $E_{vdW}^{P-S}$ ) is compensated by the sum of two repulsive solvent interactions energies ( $E_{vdW}^{W-(P+S)} = E_{vdW}^{W-S} + E_{vdW}^{W-P}$ ). This can be thought as the energy gained in adsorbing the protein is expended in breaking the hydration layers, separating it from the surface, and thus,  $\Delta_t E_{vdW}^{P-S} + \Delta_t E_{vdW}^{W-(P+S)} \approx 0$ . As a result, it follows that the vdW component of the effective adsorption force is zero (i.e.,  $F_{vdW}^{eff} = 0$ ). This result leads to an apparent contradiction, as on one hand, the adsorption is spontaneous (as shown by the CSA in Figure 4c), and on the other hand, the enthalpic vdW energy balance is null. To solve this paradox, we must now consider the entropic contribution to the adsorption energy.

Although we do not explicitly quantify this contribution, it is considered in our MD simulations, as these simulations sample the whole phase space of the system. The thermal vibrations of the water molecules allow for a protein to diffuse while in solution. Additionally, given the isotropic nature of the medium in this diffusion, statistically no direction is privileged with respect to other. If we now consider a case where an adsorbing

substrate breaks this isotropy, we may argue that this diffusion will privilege displacements toward the surface even if the enthalpic energy gain is null. The mechanism by which this occurs can be thought as follows. Let us consider a protein surrounded by water molecules in the vicinity of a substrate as shown in Figure 4d. The force felt by the protein is a sum of an attractive interaction with the surface (i.e.,  $F_{vdW}^{P-S}$ ) with a force opposing the squeezing out of solvent (i.e.,  $F_{vdW}^{W-(P+S)}$ ) necessary for the adsorption to occur. Although our MD simulations indicate that these two compensate each other, the solvent thermal fluctuations lead to temporary force unbalances. As schematically shown in Figure 4d, these unbalances can lead to a squeeze-out of the solvent and subsequent approximation of the protein toward the substrate. Additionally, it implies that the adsorption process using explicit solvent happens as a consequence of a subtle effect (i.e., the slight separation of water molecules from the protein surface as a result of thermal oscillations). Therefore, a slow approach of the protein to the surface is expected when using explicit solvent, from which follows a slow evolution of the CSA.

In order to understand why in implicit solvent MD the CSA evolution is much faster than in explicit solvent MD, we focus on the vdW solute–solvent interactions of the former. As mentioned in Sec 3.2, these interactions are included in implicit solvent simulations via the non-electrostatic solvation component (i.e.,  $E_{SOL(nonelect)}$ ), whose contribution to the total energy is negligible as compared to the  $E_{vdW}^{P-S}$ . This is at odds with the fact that vdW interactions are nonspecific. From this property, it follows that the vdW interaction force with its surroundings should be about the same either if it is in contact with the surface or with the solvent, assuming that the total area enclosing the protein is constant during the process. Although this does seem to be the case in explicit solvent simulations, this is not so for implicit solvent, because  $\Delta E_{SOL(nonelect)} + \Delta E_{vdW}^{P-S} \approx \Delta E_{vdW}^{P-S} \neq 0$  as shown in Sec. 3.2. Therefore,  $E_{SOL(nonelect)}$  is unable to describe the important vdW solvent contribution to the total energy during the adsorption process, which could be associated with processes such as the cost of breaking the solvation shells surrounding the protein and the substrate. Moreover, this also results in an overestimation of the effective adsorption force in implicit solvent simulations as  $F_{vdW}^{W-(P+S)} \approx 0$ , and thus,  $F_{vdW}^{eff} \approx F_{vdW}^{P-S}$ . This overestimation has two direct consequences: a quasi-instantaneous adsorption process and a much higher adsorption force as compared with that of explicit solvent simulations. This two consequences allow us to explain the two differences observed between implicit and explicit solvent results in the CSA evolution (i.e., faster evolution and the larger final absolute values). Moreover, although both aforementioned consequences certainly affect the protein stability, the rapid change of the CSA alone does not suffice to explain the unfolding observed in implicit solvent simulations. As explained in the following section, this quasi-instantaneous adsorption is accompanied by an abrupt change in the protein's electrostatic energy, which is ultimately the mechanism that promotes its unfolding.

**3.4. Electrostatic Interaction: Implicit Solvent Simulation Does Not Correctly Shield the Internal Energy of the Protein Adsorbed.** The previous section highlights the importance of the vdW energy component of the solvation energy in compensating the large protein–surface interaction. In what follows, we focus on the time evolution of the electrostatic component of the solvation energy (i.e.,  $\Delta_t E_{el}^{SOL}$ ) for both explicit and implicit solvent methods (Figure 5a). This energy contribution is defined as the difference between the electro-

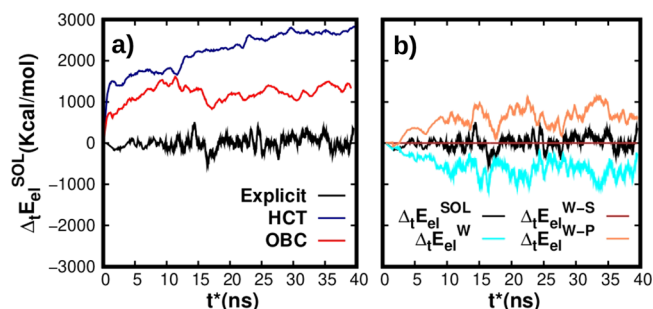


**Figure 5.** Variation of the electrostatic contribution to the solvation energy during our MD simulations ( $\Delta_t E_{el}^{SOL}$ ). (a) Using the three solvent methods considered here: HCT implicit<sup>40</sup> solvent (blue), OBC implicit<sup>41</sup> solvent (red), and explicit solvent<sup>55</sup> (black). (b) Using explicit solvent (black line), with the contribution of each of the energy components of  $E_{el}^{SOL}$ :  $E_{el}^W$  (cyan),  $E_{el}^{W-P}$  (orange), and  $E_{el}^{W-S}$  (brown).

static energy of the protein–substrate system immersed in water with respect to its electrostatic energy in vacuum.<sup>52</sup> In implicit solvent simulations, this energy component is defined as the generalized Born solvation energy.

$$E_{el}^{SOL,implicit} = E_{SOL(el)} = E_{GB} \quad (9)$$

For our system, as the graphene atoms are not charged, this term accounts for the solvent screening of the protein intramolecular electrostatic interactions. In explicit solvent simulations, the definition<sup>52</sup> of  $E_{el}^{SOL}$  results in the following expression

$$E_{el}^{SOL,explicit} = E_{el}^W + E_{el}^{W-P} + E_{el}^{W-S} \quad (10)$$

where  $E_{el}^W$  accounts for the electrostatic internal energy of the water,  $E_{el}^{W-P}$  accounts for the electrostatic water–protein interaction, and  $E_{el}^{W-S}$  accounts for the electrostatic water–surface interaction. Note that as the graphene atoms are not charged,  $E_{el}^{W-S} = 0$ .

From Figure 5a, we observe that, in explicit solvent simulations, the electrostatic contribution of the solvent energy hardly changes during the adsorption process, as  $\Delta_t E_{el}^{SOL} \approx 0$ . To analyze in detail this result, in Figure 5b, we have decomposed the evolution of  $E_{el}^{SOL}$  into its different non-null components (i.e.,  $E_{el}^W$  and  $E_{el}^{W-P}$ ). From this Figure, we may derive two different results. First, the electrostatic protein–water interaction does not favor the adsorption, as  $\Delta_t E_{el}^{W-P} > 0$ . Second,  $\Delta_t E_{el}^{W-P}$  is strongly correlated with  $\Delta_t E_{el}^W$ , as during the whole adsorption process,  $\Delta E_{el}^W \approx -\Delta E_{el}^{W-P}$ . These two results indicate that while the protein adsorbs, the loss of water–protein electrostatic energy arising from protein's dehydration is fully compensated by the gain of water's internal electrostatic energy. This internal energy gain is in turn a result of new water–water hydrogen bonds being formed during protein's dehydration. The balance between these two mechanisms explains why  $E_{el}^{SOL}$  does not seem to contribute enthalpically to the adsorption process. Moreover, this balance seems to be independent of the hydrophobic character of the protein, as a similar result is obtained for the more hydrophilic BSA protein (Figure S10). Additionally, it is important to remark that  $\Delta_t E_{el}^W$  is much smaller for the BSA adsorption as compared to the IgG's adsorption. This result is in agreement with one's expectations based on the proteins' different degrees of hydrophobicity. In particular, one would expect that the BSA (more hydrophilic) disrupts less the hydrogen-bonded water network than the IgG (less hydrophilic, see Figure S10). Therefore, during the adsorption dehydration

process, this should translate into a smaller water internal energy gain (i.e.,  $\Delta E_{el}^W$ ) in the BSA as compared with the IgG.

In Sec 3.3, we showed that in implicit solvent simulations, the protein adsorbs instantly due to a high protein–surface vdW interaction. This fast adsorption results in a rapid increase of the CSA during the first 2.5 ns for both implicit solvent methods (Figure 6a). Additionally, in Figure 6b, we also observe that

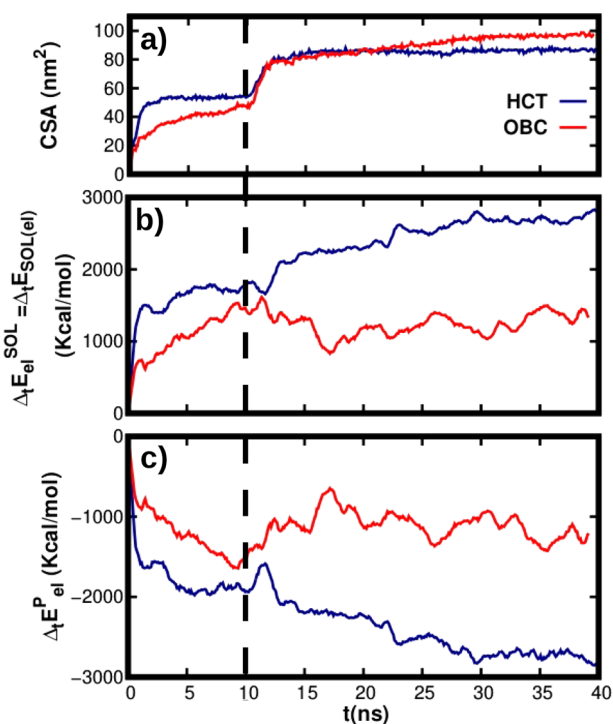


**Figure 6.** Correlation between the solvent electrostatic screening and the internal electrostatic energy of the protein. Time evolution during the whole adsorption process of (a) the CSA, (b) the electrostatic component of the solvation energy,  $E_{SOL(el)}$ , and (c) the internal electrostatic energy of the protein,  $E_{el}^P$ , using the HCT<sup>40</sup> (blue) and the OBC<sup>41</sup> (red) implicit solvent methods.

during this time range,  $\Delta E_{el}^{SOL} > 700$  kcal/mol, which shows that the electrostatic contribution of the solvent energy is working against the protein adsorption, thus acting as an effective repulsive force. However, this *repulsive* force is unable to hinder the protein adsorption, as the attractive vdW protein–surface interaction compensates this energy loss (Figure 3a). Still, as a result of the adsorption, the system is left with a large electrostatic energy unbalance, which may only be alleviated by a major structural rearrangement of the charges present on the system, which in implicit solvent is only on the protein atoms. Remarkably, in Figure 6c, we observe that the protein’s internal electrostatic energy,  $E_{el}^P$ , not only decreases significantly as a result of the adsorption process but also the variation of this energy component is strongly correlated with  $\Delta E_{el}^{SOL}$ . This correlation demonstrates that the aforementioned electrostatic unbalance leads to a major protein-structural rearrangement. Moreover, it is important to note that all these energy changes (namely,  $\Delta E_{el}^P$ ,  $\Delta E_{el}^{SOL}$ , and  $\Delta E_{vdW}^P$ ) occur almost instantaneously (i.e., within the first two nanoseconds). The large energy unbalances coupled with their fast time rates result in a swift protein unfolding upon adsorption when using implicit solvent methods, as clearly evidenced by its secondary structure evolution shown in Figure 2d. Therefore, protein adsorption

using implicit-solvation methods can be seen as a three step process. First, the protein quickly approaches the surface as a consequence of the vdW interaction. Second, as a consequence of the protein–surface approach, a large electrostatic repulsive force emerges from the solvent contribution. Lastly, to reduce that this energy unbalance, the protein is *instantaneously* forced to rearrange its atoms, which in turn leads to the protein’s unfolding. As a result, one may argue that this spurious unfolding observed in many different implicit solvent MD works concerning the protein adsorption to uncharged surfaces may be understood in terms of the ill-characterization of these three elements.

One of the two major differences observed between implicit and explicit solvent MD simulations concerns the evolution of the electrostatic energy component of the solvation energy. In particular, Figure 5a shows that  $\Delta E_{el}^{SOL,implicit} > 0$ , whereas  $\Delta E_{el}^{SOL,explicit} \approx 0$ . This major qualitative and quantitative difference may be traced back to the definition of this term in the two solvent methods (eqs 9 and 10). In the explicit solvent simulation,  $\Delta E_{el}^{SOL,explicit}$  considers two different solvent effects: the changes in protein’s intramolecular solvent screening via the  $\Delta E_{el}^{W-P}$  term and the changes in the solvent–solvent electrostatic interaction via the  $\Delta E_{el}^W$  term. Notably, in Figure 5b, we observed that these two terms are highly correlated. This correlation highlights the feedback mechanism, in which electrostatic energy losses arising from protein’s dehydration are compensated by similar energy gains in the solvent (through, e.g., additional solvent–solvent hydrogen bonds). This balance loss/gain of electrostatic interactions of the water molecules with protein/water is what ultimately regulates the electrostatic contribution of the solvation energy, leading to  $\Delta E_{el}^{SOL,explicit} \approx 0$  during adsorption. However, in implicit solvent simulations,  $\Delta E_{el}^{SOL,implicit}$  only accounts for the first of this two effects (i.e., the loss of the solvent screening of the intramolecular protein electrostatic interactions). For this reason, using this solvent method, the electrostatic contribution to the solvent energy supposes a positive energy gradient ( $\Delta E_{el}^{SOL,implicit} > 0$ ), which only can be balanced with the reorganization of the protein’s atoms. This difference remarks the importance of considering the gain of the water–water electrostatic interaction during adsorption, as only when it is omitted (implicit solvent), the evolution of  $E_{el}^{SOL}$  affects the structural stability of the protein.

The other difference between implicit and explicit solvent simulations concerns the loss of the water–protein electrostatic interaction while the protein adsorbs/dehydrates. To understand this difference, we first need to comprehend how  $E_{el}^{SOL,implicit}$  describes this process. To this aim, we have analyzed the variation of  $E_{el}^{SOL,implicit}$  when a charged model molecule approaches a neutral model surface. Both systems (i.e., the molecule and the surface), are conformed by spheres/atoms of radius  $1 R_{vdW}$ , as shown in the inset of Figure 7a. The spheres of the molecule are equally positively charged, whereas the ones of the surface are neutral. We have used the same definition of  $E_{el}^{SOL,implicit} = E_{SOL(el)} = E_{GB}$  as in the HCT method<sup>40</sup> (eq 2). According to that definition, each charged sphere/atom  $i$  of the solute contributes to the total electrostatic component of the solvent energy via the expression

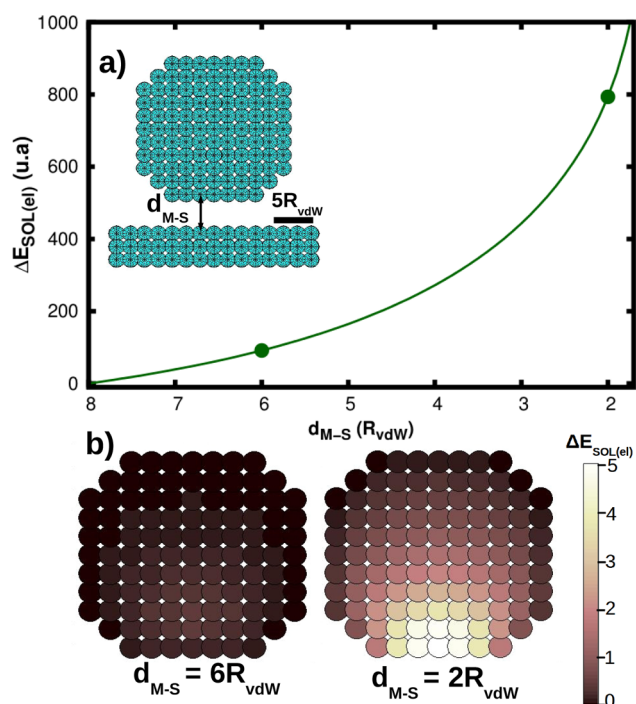


**Figure 7.** Modeling the loss of the solvent electrostatic screening predicted by implicit solvent methods. (a) Change of the electrostatic component of the solvent energy,  $E_{SOL(el)}$ , when the distance between the model molecule and surface ( $d_{M-S}$ ) decreases. The model molecule is conformed by 852 positively charged spheres, and the surface is formed by 667 neutral spheres distributed in three layers. The radius of all the spheres is  $1 R_{vdW}$ . A representation of the whole system is showed in the inset. (b)  $\Delta E_{SOL(el)}$  per sphere when  $d_{M-S} = 6 R_{vdW}$  (left) and  $d_{M-S} = 2 R_{vdW}$  (right).

$$\begin{aligned}
 E_{SOL(el)} &= \sum_i E_{SOL(el)}(i) \\
 &= -\left(\frac{\epsilon_\omega - 1}{2\epsilon_\omega}\right) \sum_i \sum_j \frac{q_i q_j}{r_{ij} \sqrt{1 + \frac{R_i R_j}{r_{ij}^2} e^{-r_{ij}^2/4R_i R_j}}}
 \end{aligned}
 \quad (11)$$

where  $R_i$  (i.e., the effective Born radii), reflects the degree of burial of the sphere/atom  $i$  inside the molecule. We have computed numerically that expression to analyze how  $E_{SOL(el)}$  changes with the molecule–surface distance,  $d_{M-S}$ .

In Figure 7a, we observe that, as the molecule approaches to the surface,  $E_{SOL(el)}$  largely increases. This result is very similar to the one shown in Figure 3a (i.e., when the molecule and the surface are the IgG protein and the graphene double layer, respectively). This similarity highlights that the observed increase of  $E_{SOL(el)}$  during adsorption is not a specific consequence of the adsorption process of the IgG but a general feature of the implicit solvent methods. To understand this feature, we analyze the contribution of each molecule’s sphere to  $\Delta E_{SOL(el)}$  for different  $d_{M-S}$  values. In Figure 7b, we observe an enhancement of the contribution of the spheres closer to the surface when  $d_{M-S}$  decreases. This enhancement, in accordance with eq 11, arises from an increase of the Born radii of these “close to surface” spheres as shown in Figure S11. Therefore, the increase of  $E_{SOL(el)}$  when a charged molecule approaches a neutral surface accounts for the following process. When the molecule is far from the surface, the degree of burial of one molecule sphere only depends on its position inside the

molecule. For this reason, these “close to surface” spheres/atoms are outer spheres in that situation (small Born radii). However, when the molecule approaches to the surface, the position of the surface spheres starts to affect the degree of burial of the molecule spheres. As a consequence, these “close to surface” spheres/atoms start to act as inner spheres (i.e., their Born radii enlarge). This ultimately leads to the increase of  $E_{SOL(el)}$ , explaining how the loss of water–protein electrostatic interactions is described in implicit solvent simulations.

In an explicit solvent simulation, the loss of water–protein electrostatic interactions is described via the removal of the water molecules that are in the region between the molecule and the surface. This removal process is more gradual than the process of change of the Born radii used in implicit solvent simulations. Additionally, as implicit solvent methods overestimate the effective vdW protein–surface attractive force, the adsorption process is faster in these simulations than in those using explicit solvent (Sec 3.3). These two factors cause, as shown in Figure 5, a larger and faster loss of water–protein electrostatic interaction in implicit solvent simulation ( $\Delta E_{el}^{SOL,implicit}$ ) than in explicit solvent simulations ( $\Delta E_{el}^{W-P}$ ). Considering the direct correlation between this loss and the reorganization of the protein’s atoms, this difference is translated into instantaneous and great changes in the structure of the protein. Therefore, the abrupt loss of water–protein electrostatic interactions contributes also to the unfolding of the protein.

#### 4. CONCLUSIONS

In this work, the IgG adsorption process on a graphene surface was studied using both explicit and implicit solvent simulations. The results of the explicit solvent simulation show that water molecules play an active role in the adsorption process. When the protein approaches the graphene surface, the loss of water–protein electrostatic interaction becomes balanced by the gain of the water–water electrostatic interaction. This regulates the electrostatic contribution of the solvation energy. Additionally, the cost of breaking protein and surface solvation shells compensates the vdW attraction that exists between them. Despite this energy compensation, the protein adsorbs on the surface. This indicates that the driving force of the adsorption process does not only present an enthalpic origin. The thermal vibrations of the water molecules allow the protein to diffuse, and the presence of an attractive protein–surface force guides this protein diffusion toward the surface. Therefore, entropic effects seem to be important in the adsorption process of a protein on a neutral surface.

In contrast, implicit solvent methods underestimate the cost of breaking the solvation shells of the protein and the substrate. This leads to an overestimation of the effective vdW protein–surface attractive force, causing an instantaneous adsorption process. In addition to the fast adsorption process, a large energy gradient arises from the loss of the water–protein electrostatic interaction. Contrary to explicit solvent simulation, that energy gradient is not balanced by the gain of water–water electrostatic interaction, which is not included in implicit solvent simulations. Therefore, the only way of alleviating that energy unbalance is by reorganizing the position of the only charges of the system, the protein atoms. This reorganization happens abruptly, which leads to the unfolding of the protein. Thus, in this work, we have been able to understand the factors that lead to unfolded protein configuration upon adsorption when implicit solvent methods are used. To evade the unfolding of the protein, we propose to

improve both non-electrostatic and electrostatic components of the solvation energy. Concerning the first, we think that it underestimates the vdW repulsive solute–solvent interaction, which according to explicit solvent simulations has an important role in the adsorption process. Regarding the electrostatic component, we propose a correction in the Born radii definition in order to obtain a more gradual loss of the solvent screening of the intraprotein electrostatic interactions.

## ■ ASSOCIATED CONTENT

### 📄 Supporting Information

The Supporting Information is available free of charge on the ACS Publications website at DOI: [10.1021/acs.jctc.8b01060](https://doi.org/10.1021/acs.jctc.8b01060).

Further details concerning: (i) the protein-structural dynamics free in solution and during the adsorption process; (ii) results for adsorption with a different protein orientation; (iii) tests of our simulation methodology; and (iv) the energy decomposition analysis (PDF)

## ■ AUTHOR INFORMATION

### Corresponding Authors

\*E-mail: [guilhermivilhena@gmail.com](mailto:guilhermivilhena@gmail.com). (J.G.V.)

\*E-mail: [ruben.perez@uam.es](mailto:ruben.perez@uam.es). (R.P.)

### ORCID

J. G. Vilhena: 0000-0001-8338-9119

Rubén Pérez: 0000-0001-5896-541X

### Notes

The authors declare no competing financial interest.

## ■ ACKNOWLEDGMENTS

We acknowledge financial support from the Spanish MINECO (projects CSD2010-00024, FIS2015-69295-C3-1-P, MDM-2014-0377, MAT2014-54484-P, and MAT2017-83273-R). J.G.V. acknowledges funding from a Marie Skłodowska-Curie Fellowship within the Horizons 2020 framework (DLV-795286). The authors thankfully acknowledge the computer resources, technical expertise, and assistance provided by the Red Española de Supercomputación (RES) at the Minotauro and Marenostrum supercomputers (BSC, Barcelona). We also acknowledge the Extremadura Research Centre for Advanced Technologies (CETA-CIEMAT).

## ■ REFERENCES

- (1) Norde, W.; Horbett, T. A.; Brash, J. L. *Proteins at Interfaces III State of the Art*; ACS Symposium Series; American Chemical Society, 2012; Vol. 1120, pp 1–34.
- (2) Rabe, M.; Verdes, D.; Seeger, S. Understanding protein adsorption phenomena at solid surfaces. *Adv. Colloid Interface Sci.* **2011**, *162*, 87–106.
- (3) Sanhai, W. R.; Sakamoto, J. H.; Canady, R.; Ferrari, M. Seven Challenges for Nanomedicine. *Nat. Nanotechnol.* **2008**, *3*, 242–244.
- (4) Zhang, Z.; Zhang, M.; Chen, S.; Horbett, T. A.; Ratner, B. D.; Jiang, S. Blood Compatibility of Surfaces With Superlow Protein Adsorption. *Biomaterials* **2008**, *29*, 4285–4291.
- (5) Yanik, A. A.; Huang, M.; Kamohara, O.; Artar, A.; Geisbert, T. W.; Connor, J. H.; Altug, H. An Optofluidic Nanoplasmic Biosensor for Direct Detection of Live Viruses from Biological Media. *Nano Lett.* **2010**, *10*, 4962–4969.
- (6) Herruzo, E. T.; Asakawa, H.; Fukuma, T.; Garcia, R. Three-dimensional quantitative force maps in liquid with 10 piconewton, angstrom and sub-minute resolutions. *Nanoscale* **2013**, *5*, 2678–2685.

(7) Kuchuk, K.; Sivan, U. Hydration Structure of a Single DNA Molecule Revealed by Frequency-Modulation Atomic Force Microscopy. *Nano Lett.* **2018**, *18*, 2733–2737.

(8) Höök, F.; Vörös, J.; Rodahl, M.; Kurrat, R.; Böni, P.; Ramsden, J.; Textor, M.; Spencer, N.; Tengvall, P.; Gold, J.; Kasemo, B. A comparative study of protein adsorption on titanium oxide surfaces using in situ ellipsometry, optical waveguide lightmode spectroscopy, and quartz crystal microbalance/dissipation. *Colloids Surf., B* **2002**, *24*, 155–170.

(9) Geisler, M.; Xiao, S.; Puchner, E. M.; Gräter, F.; Hugel, T. Controlling the Structure of Proteins at Surfaces. *J. Am. Chem. Soc.* **2010**, *132*, 17277–17281.

(10) Pelaz, B.; del Pino, P.; Maffre, P.; Hartmann, R.; Gallego, M.; Rivera-Fernández, S.; de la Fuente, J. M.; Nienhaus, G. U.; Parak, W. J. Surface Functionalization of Nanoparticles with Polyethylene Glycol: Effects on Protein Adsorption and Cellular Uptake. *ACS Nano* **2015**, *9*, 6996–7008.

(11) Sharma, I.; Pattanayek, S. K. Effect of surface energy of solid surfaces on the micro- and macroscopic properties of adsorbed BSA and lysozyme. *Biophys. Chem.* **2017**, *226*, 14–22.

(12) Latour, R. A. Molecular simulation of protein-surface interactions: Benefits, problems, solutions, and future directions (Review). *Biointerphases* **2008**, *3*, FC2–FC12.

(13) Penna, M. J.; Mijajlovic, M.; Biggs, M. J. Molecular-Level Understanding of Protein Adsorption at the Interface between Water and a Strongly Interacting Uncharged Solid Surface. *J. Am. Chem. Soc.* **2014**, *136*, 5323–5331.

(14) Gray, J. J. The interaction of proteins with solid surfaces. *Curr. Opin. Struct. Biol.* **2004**, *14*, 110–115.

(15) Latour, R. A. In *Biological Interactions on Materials Surfaces: Understanding and Controlling Protein, Cell, and Tissue Responses*; Puleo, D. A., Bizios, R., Eds.; Springer: New York, 2009; pp 69–95.

(16) Feig, M.; Brooks, C. L. Recent Advances in the Developments and Application of Implicit Solvent Models in Biomolecule Simulations. *Curr. Opin. Struct. Biol.* **2004**, *14*, 217–224.

(17) Luo, R.; David, L.; Gilson, M. K. Accelerated Poisson-Boltzmann calculations for static and dynamic systems. *J. Comput. Chem.* **2002**, *23*, 1244–1253.

(18) Still, W. C.; Tempczyk, A.; Hawley, R. C.; Hendrickson, T. Semianalytical treatment of solvation for molecular mechanics and dynamics. *J. Am. Chem. Soc.* **1990**, *112*, 6127–6129.

(19) Born, M. Volumen und Hydratationswärme der Ionen. *Eur. Phys. J. A* **1920**, *1*, 45–48.

(20) Onufriev, A.; Case, D. A.; Bashford, D. Effective Born radii in the generalized Born approximation: The importance of being perfect. *J. Comput. Chem.* **2002**, *23*, 1297–1304.

(21) Feig, M.; Onufriev, A.; Lee, M.; Im, W.; Case, D. A.; Brooks, C. L. Performance Comparison of the Generalized Born and Poisson Methods in the Calculation of the Electrostatic Solvation Energies for Protein Structures. *J. Comput. Chem.* **2004**, *25*, 265–284.

(22) Ferrara, P.; Apostolakis, J.; Caflisch, A. Evaluation of a fast implicit solvent model for molecular dynamics simulations. *Proteins: Struct., Funct., Genet.* **2002**, *46*, 24–33.

(23) Orozco, M.; Luque, F. J. Theoretical Methods for the Description of the Solvent Effect in Biomolecular Systems. *Chem. Rev.* **2000**, *100*, 4187–4226.

(24) Gohlke, H.; Case, D. A. Converging free energy estimates: MM-PB(GB)SA studies on the protein-protein complex Ras-Raf. *J. Comput. Chem.* **2004**, *25*, 238–250.

(25) Kleinjung, J.; Fraternali, F. Design and application of implicit solvent models in biomolecular simulations. *Curr. Opin. Struct. Biol.* **2014**, *25*, 126–134. Theory and simulation/macromolecular machines.

(26) Arnaudova, Y. A.; Vorobjev, Y. N.; Vila, J. A.; Scheraga, H. A. Identifying natively like protein structures with scoring functions based on all-atom ECEPP force fields, implicit solvent models and structure relaxation. *Proteins: Struct., Funct., Genet.* **2009**, *77*, 38–51.

(27) Al Qaraghuli, M. M.; Kubiak-Ossowska, K.; Mulheran, P. A. Thinking outside the Laboratory: Analyses of Antibody Structure and

Dynamics within Different Solvent Environments in Molecular Dynamics (MD) Simulations. *Antibodies* **2018**, *7*, 21.

(28) Raffaini, G.; Ganazzoli, F. Surface Topography Effects in Protein Adsorption on Nanostructured Carbon Allotropes. *Langmuir* **2013**, *29*, 4883–4893.

(29) Raffaini, G.; Ganazzoli, F. Protein Adsorption on a Hydrophobic Surface: A Molecular Dynamics Study of Lysozyme on Graphite. *Langmuir* **2010**, *26*, 5679–5689.

(30) Raffaini, G.; Ganazzoli, F. Understanding the Performance of Biomaterials through Molecular Modeling: Crossing the Bridge between their Intrinsic Properties and the Surface Adsorption of Proteins. *Macromol. Biosci.* **2007**, *7*, 552–566.

(31) Ganazzoli, F.; Raffaini, G. Computer Simulation of Polypeptide Adsorption on Model Biomaterials. *Phys. Chem. Chem. Phys.* **2005**, *7*, 3651–3663.

(32) Raffaini, G.; Ganazzoli, F. Simulation Study of the Interaction of Some Albumin Subdomains With a Flat Graphite Surface. *Langmuir* **2003**, *19*, 3403–3412.

(33) Mücksch, C.; Urbassek, H. M. Adsorption of BMP-2 on a Hydrophobic Graphite Surface: A Molecular Dynamics Study. *Chem. Phys. Lett.* **2011**, *510*, 252–256.

(34) Mücksch, C.; Urbassek, H. M. Enhancing Protein Adsorption Simulations by Using Accelerated Molecular Dynamics. *PLoS One* **2013**, *8*, No. e64883.

(35) Horinek, D.; Serr, A.; Geisler, M.; Pirzer, T.; Slotta, U.; Lud, S. Q.; Garrido, J. A.; Scheibel, T.; Hugel, T.; Netz, R. R. Peptide Adsorption on a Hydrophobic Surface Results from an Interplay of Solvation, Surface, and Intrapeptide Forces. *Proc. Natl. Acad. Sci. U. S. A.* **2008**, *105*, 2842–2847.

(36) Wei, T.; Carignano, M. A.; Szleifer, I. Lysozyme Adsorption on Polyethylene Surfaces: Why Are Long Simulations Needed? *Langmuir* **2011**, *27*, 12074–12081.

(37) Ou, L.; Luo, Y.; Wei, G. Atomic-Level Study of Adsorption, Conformational Change, and Dimerization of an  $\alpha$ -Helical Peptide at Graphene Surface. *J. Phys. Chem. B* **2011**, *115*, 9813–9822.

(38) Wei, T.; Carignano, M. A.; Szleifer, I. Molecular Dynamics Simulation of Lysozyme Adsorption/Desorption on Hydrophobic Surfaces. *J. Phys. Chem. B* **2012**, *116*, 10189–10194.

(39) Vilhena, J. G.; Dumitru, A. C.; Herruzo, E. T.; Mendieta-Moreno, J. I.; Garcia, R.; Serena, P. A.; Perez, R. Adsorption Orientations and Immunological Recognition of Antibodies on Graphene. *Nanoscale* **2016**, *8*, 13463–13475.

(40) Hawkins, G. D.; Cramer, C. J.; Truhlar, D. G. Parametrized Models of Aqueous Free Energies of Solvation Based on Pairwise Descreening of Solute Atomic Charges From a Dielectric Medium. *J. Phys. Chem.* **1996**, *100*, 19824–19839.

(41) Onufriev, A.; Bashford, D.; Case, D. A. Exploring Protein Native States and Large-Scale Conformational Changes With a Modified Generalized Born Model. *Proteins: Struct., Funct., Genet.* **2004**, *55*, 383–394.

(42) Connolly, M. L. Analytical Molecular Surface Calculation. *J. Appl. Crystallogr.* **1983**, *16*, 548–558.

(43) Harris, L. J.; Larson, S. B.; Hasel, K. W.; McPherson, A. Refined Structure of an Intact IgG2a Monoclonal Antibody. *Biochemistry* **1997**, *36*, 1581–1597.

(44) Gordon, J. C.; Myers, J. B.; Folta, T.; Shoja, V.; Heath, L. S.; Onufriev, A. H++: a Server for Estimating pKas and Adding Missing Hydrogens to Macromolecules. *Nucleic Acids Res.* **2005**, *33*, W368–W371.

(45) Lindorff-Larsen, K.; Piana, S.; Palmo, K.; Maragakis, P.; Klepeis, J. L.; Dror, R. O.; Shaw, D. E. Improved Side-Chain Torsion Potentials for the Amber ff99SB Protein Force Field. *Proteins: Struct., Funct., Genet.* **2010**, *78*, 1950–1958.

(46) Kirschner, K. N.; Yongye, A. B.; Tschampel, S. M.; González-Outeiriño, J.; Daniels, C. R.; Foley, B. L.; Woods, R. J. GLYCAM06: A generalizable biomolecular force field. *Carbohydrates. J. Comput. Chem.* **2008**, *29*, 622–655.

(47) Brandt, J. P.; Patapoff, T. W.; Aragon, S. R. Construction, MD Simulation, and Hydrodynamic Validation of an All-Atom Model of a Monoclonal IgG Antibody. *Biophys. J.* **2010**, *99*, 905–913.

(48) Wang, J.; Wolf, R. M.; Caldwell, J. W.; Kollman, P. A.; Case, D. A. Development and Testing of a General Amber Force Field. *J. Comput. Chem.* **2004**, *25*, 1157–1174.

(49) Tsai, J.-L.; Tu, J.-F. Characterizing Mechanical Properties of Graphite Using Molecular Dynamics Simulation. *Mater. Eng.* **2010**, *31*, 194–199.

(50) Pykal, M.; Jurecka, P.; Karlicky, F.; Otyepka, M. Modelling of graphene functionalization. *Phys. Chem. Chem. Phys.* **2016**, *18*, 6351–6372.

(51) Vilhena, J. G.; Pimentel, C.; Pedraz, P.; Luo, F.; Serena, P. A.; Pina, C. M.; Gnecco, E.; Pérez, R. Atomic-Scale Sliding Friction on Graphene in Water. *ACS Nano* **2016**, *10*, 4288–4293.

(52) Onufriev, A.; Bashford, D.; Case, D. A. Modification of the Generalized Born Model Suitable for Macromolecules. *J. Phys. Chem. B* **2000**, *104*, 3712–3720.

(53) Hawkins, G. D.; Cramer, C. J.; Truhlar, D. G. Pairwise Solute Descreening of Solute Charges from a Dielectric Medium. *Chem. Phys. Lett.* **1995**, *246*, 122–129.

(54) Liu, H.; Chen, F.; Sun, H.; Li, D.; Hou, T. Improving the Efficiency of Non-equilibrium Sampling in the Aqueous Environment via Implicit-Solvent Simulations. *J. Chem. Theory Comput.* **2017**, *13*, 1827–1836.

(55) Jorgensen, W. L.; Chandrasekhar, J.; Madura, J. D.; Impey, R. W.; Klein, M. L. Comparison of Simple Potential Functions for Simulating Liquid Water. *J. Chem. Phys.* **1983**, *79*, 926–935.

(56) Case, D. A.; Darden, T. A.; Simmerling, C.; Wang, J.; Duke, R.; Luo, R.; Walker, R.; Zhang, W.; Merz, K.; Roberts, B.; Hayik, S.; Roitberg, A.; Seabra, G.; Swails, J.; Gtz, A.; Kolossvy, I.; Wong, K.; Paesani, F.; Vanicek, J.; Wolf, R.; Liu, J.; Wu, X.; Brozell, S.; Steinbrecher, T.; Gohlke, H.; Cai, Q.; Ye, X.; Wang, J.; Hsieh, M.-J.; Cui, G.; Roe, D.; Mathews, D.; Seetin, M.; Salomon-Ferrer, R.; Sagui, C.; Babin, V.; Luchko, T.; Gusarov, S.; Kovalenko, A.; Kollman, P. *AMBER 12*; University of California: San Francisco, 2012.

(57) Götz, A. W.; Williamson, M. J.; Xu, D.; Poole, D.; Le Grand, S.; Walker, R. C. Routine Microsecond Molecular Dynamics Simulations with AMBER on GPUs. 1. Generalized Born. *J. Chem. Theory Comput.* **2012**, *8*, 1542–1555.

(58) Salomon-Ferrer, R.; Götz, A. W.; Poole, D.; Le Grand, S.; Walker, R. C. Routine Microsecond Molecular Dynamics Simulations with AMBER on GPUs. 2. Explicit Solvent Particle Mesh Ewald. *J. Chem. Theory Comput.* **2013**, *9*, 3878–3888.

(59) Crowley, M.; Darden, T.; Cheatham, T., III; Deerfield, D., II. Adventures in Improving the Scaling and Accuracy of a Parallel Molecular Dynamics Program. *Journal of Supercomputing* **1997**, *11*, 255–278.

(60) Essmann, U.; Perera, L.; Berkowitz, M. L.; Darden, T.; Lee, H.; Pedersen, L. G. A smooth particle mesh Ewald method. *J. Chem. Phys.* **1995**, *103*, 8577–8593.

(61) Miyamoto, S.; Kollman, P. A. Settle: An analytical version of the SHAKE and RATTLE algorithm for rigid water models. *J. Comput. Chem.* **1992**, *13*, 952–962.

(62) Loncharich, R. J.; Brooks, B. R.; Pastor, R. W. Langevin dynamics of peptides: The frictional dependence of isomerization rates of N-acetylalanine-N-methylamide. *Biopolymers* **1992**, *32*, 523–535.

(63) Berendsen, H. J. C.; Postma, J. P. M.; van Gunsteren, W. F.; DiNola, A.; Haak, J. R. Molecular dynamics with coupling to an external bath. *J. Chem. Phys.* **1984**, *81*, 3684–3690.

(64) Rogge, S.; Vanduyfhuys, L.; Ghysels, A.; Waroquier, M.; Verstraelen, T.; Maurin, G.; Van Speybroeck, V. A Comparison of Barostats for the Mechanical Characterization of Metal/Organic Frameworks. *J. Chem. Theory Comput.* **2015**, *11*, 5583–5597.

(65) Allen, M. P.; Tildesley, D. J. *Computer simulation of liquids*, 2nd ed.; Oxford University Press, 2017.

(66) Roe, D. R.; Cheatham, T. E. PTRAJ and CPPTRAJ: Software for Processing and Analysis of Molecular Dynamics Trajectory Data. *J. Chem. Theory Comput.* **2013**, *9*, 3084–3095.

(67) Kabsch, W.; Sander, C. Dictionary of Protein Secondary Structure: Pattern Recognition of Hydrogen-Bonded and Geometrical Features. *Biopolymers* **1983**, *22*, 2577–2637.

(68) Joosten, R. P.; te Beek, T. A. H.; Krieger, E.; Hekkelman, M. L.; Hooft, R. W. W.; Schneider, R.; Sander, C.; Vriend, G. A Series of PDB Related Databases for Everyday Needs. *Nucleic Acids Res.* **2011**, *39*, D411–D419.

(69) Vermeer, A. W.; Norde, W.; van Amerongen, A. The Unfolding/Denaturation of Immunoglobulin of Isotype 2b and its Fab and Fc Fragments. *Biophys. J.* **2000**, *79*, 2150–2154.

(70) Vilhena, J. G.; Rubio-Pereda, P.; Velloso, P.; Serena, P. A.; Pérez, R. Albumin (BSA) Adsorption over Graphene in Aqueous Environment: Influence of Orientation, Adsorption Protocol, and Solvent Treatment. *Langmuir* **2016**, *32*, 1742–1755.

(71) Raju, A. P. A.; Offerman, S. C.; Gorgojo, P.; Valles, C.; Bichenkova, E. V.; Aojula, H. S.; Vijayraghavan, A.; Young, R. J.; Novoselov, K. S.; Kinloch, I. A.; Clarke, D. J. Dispersal of Pristine Graphene for Biological Studies. *RSC Adv.* **2016**, *6*, 69551–69559.

(72) Garrett, R.; Grisham, C. *Biochemistry*, 5th ed.; Cengage Learning, 2012.